Chemical Engineering Journal 387 (2020) 124089

Contents lists available at ScienceDirect

Chemical Engineering Journal

journal homepage: www.elsevier.com/locate/cej

Interface engineering on cathode side for solid garnet batteries

Zhijie Bi[a], Ning Zhao[a], Lina Ma[b], Zhengqian Fu[c], Fangfang Xu[c], Chunsheng Wang[d,*], Xiangxin Guo[a,*]

[a] College of Physics, Qingdao University, Qingdao 266071, China
[b] College of Chemistry and Chemical Engineering, Qingdao University, Qingdao 266071, China
[c] Shanghai Institute of Ceramics, Chinese Academy of Sciences, Shanghai 200050, China
[d] Department of Chemical and Biomolecular Engineering, University of Maryland, MD 20742, United States

HIGHLIGHTS

- LLZNO nanoparticles coated $LiCoO_2$ cathodes are synthesized by a sol-gel method.
- 3D ionic/electronic conducting networks inside the cathodes are constructed.
- A reactive intermediate layer of PP13-TFSI is introduced in cathode/garnet interface.
- A solid electrolyte interphase composed of LiF, Li_3N, Li_2S and Li_2O is in situ formed.

GRAPHICAL ABSTRACT

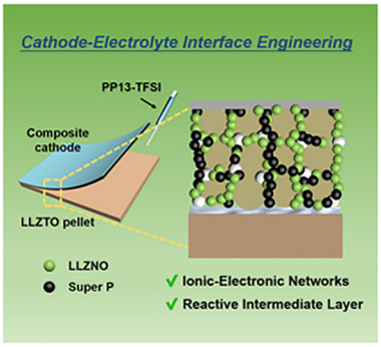

ARTICLE INFO

Keywords:
Solid-state batteries
Garnet electrolytes
$Li_{6.375}La_3Zr_{1.375}Nb_{0.625}O_{12}$ nanoparticles
Reactive interfaces
Conducting networks

ABSTRACT

The garnet solid electrolyte battery confronts crucial challenges of electronic/ionic conduction inside the cathode and interfacial contact between the cathode and the electrolyte. In this report, a super ion/electron conductive $LiCoO_2$ (LCO) material is fabricated by partially coating nano $Li_{6.375}La_3Zr_{1.375}Nb_{0.625}O_{12}$ (LLZNO) electrolyte on LCO and then filling Super P carbons into the uncoated space. This configuration offers continuous ionically and electronically conducting networks inside the LCO cathode. In addition, an intermediate layer of N-Methyl-N-propylpiperidinium bis(trifluoromethanesulfonyl)imide (PP13-TFSI) is introduced in between the composite cathode and the garnet electrolyte to form a solid-state ionically conducting interphase during charge/discharge cycles. Through the above interfacial engineering, the solid garnet batteries based on $LiCoO_2$ run as long as 400 cycles with the capacity retention of 80.2% at 0.2 C and 60 °C.

1. Introduction

The solid-sate battery becomes a rising star due to its potential in breakthrough of the energy-density limit facing by the currently commercial liquid organic lithium-ion battery [1–6]. In addition, it also avoids the safety concern on using nonflammable solid electrolytes [7–10]. However, replacement of the liquid electrolyte by the solid electrolyte also causes crucial interfacial challenges [11–16]. On the cathode side, unlike the liquid electrolyte that can maintain good contact to the porous cathode, the solid contact between the solid electrolyte, carbon, and the cathode will gradually lose due to the volume change of the cathodes, increasing the ionic and electronic

* Corresponding authors.
E-mail addresses: cswang@umd.edu (C. Wang), xxguo@qdu.edu.cn (X. Guo).

https://doi.org/10.1016/j.cej.2020.124089
Received 11 December 2019; Received in revised form 5 January 2020; Accepted 10 January 2020
Available online 11 January 2020
1385-8947/

resistance in the cathodes and reducing the capacity with charge/discharge cycles [17,18]. In addition, the intimate contact between the cathode and the solid electrolyte is also required in order to promote ion transport and thus reduce the interfacial resistance [19].

So far, many efforts have been devoted to enhance the interfacial contact in composite cathodes of solid garnet batteries. Han et al. [20] sintered Li_2CO_3 coated $LiCoO_2$ and LLZO together with the assistance of $Li_{2.3}C_{0.7}B_{0.3}O_3$ solder, realizing enhanced cathode-electrolyte interfaces. However, the sintered interfaces are rigid, which are difficult to stand large volume variation especially in the case of long-life cycling. Coating of cathodes by ionically conductive layers including less rigid $Li_{1+x}Al_xTi_{2-x}(PO_4)_3$ [21,22] or flexible polymers [23,24] offers stable contacts between active materials and electrolytes. However, continuous coating of electrolyte layers may block electronic transports. The polymers tend to decompose when charge potential is over 4 V. Furthermore, the lack of effective method to maintain good contact between the cathode and the electrolyte hinders the cycle stability of solid garnet batteries.

In this work, the micro-sized LCO particles was coated by $Li_{6.375}La_3Zr_{1.375}Nb_{0.625}O_{12}$ (LLZNO) electrolyte nanoparticles (abbreviated as LCO@LLZNO, Fig. 1a). The coverage of LLZNO nanoparticle is controlled by the amount of LLZNO. Then Super P (SP) was filled into the uncovered spaces between LLZNO nanoparticles to form three dimensional (3D) ionically and electronically conducting networks after assembling into LCO cathodes (Fig. 1b and c). In addition, N-Methyl-N-propylpiperidinium bis(trifluoromethanesulfonyl)imide (PP13-TFSI) ionic liquid (IL) was introduced in between the cathode and the electrolyte to reduce the contact resistance (Fig. 1d) because the IL has good thermal stability, nonflammable, nonvolatile properties [25–28], and may be decomposed into solid electrolyte interphase (SEI) consisting of LiF, Li_3N, Li_2S and Li_2O during charge/discharge cycles [29,30]. The SEI layer can reduce the interfacial resistance and improve the cycle stability of solid batteries. Consequently, the solid-state Li/LCO batteries with 3D ionically and electronically conducting cathodes and in situ formed SEI between cathodes and electrolytes significantly enhance the cell electrochemical performance.

2. Materials and methods

2.1. Materials synthesis

The LLZNO coated $LiCoO_2$ (LCO@LLZNO) was synthesized by a facile one-step sol-gel process. The raw cathode material $LiCoO_2$ purchased from Aladdin Reagent was used without further purification. Stoichiometric $LiNO_3$ (Aladdin Reagent, 99.9%, 10% excess was added to compensate for Li loss), $La(NO_3)_3{\cdot}6H_2O$ (Aladdin Reagent, 99.9%), $ZrOCl_2{\cdot}8H_2O$ (Aladdin Reagent, 99.99%) and $NbCl_5$ (Aladdin Reagent, 99.9%) were completely dissolved in sufficient deionized water under vigorous stirring. Citric acid monohydrate was then added, the amount of which was twice the total moles of cations in the precursor solution. Magnetic stirring was applied at 50 °C for 4 h until a transparent sol was formed. Afterwards, $LiCoO_2$ powder was immersed in a certain amount of sol (2 wt% LLZNO) followed by stirring at 50 °C for 4 h. The solvent was then gradually evaporated at 80 °C and a viscous gel was obtained. The gel containing $LiCoO_2$ cathode powder was then completely dried at 100 °C for 4 h in an oven. Subsequently, the obtained powder was calcined at 850 °C for 6 h at a muffle furnace, followed by naturally cooling to room temperature to acquire the final LCO@LLZNO. Fig. 1a schematically presents the synthesis process of sol-gel processed LCO@LLZNO cathode.

The garnet-type $Li_{6.4}La_3Zr_{1.4}Ta_{0.6}O_{12}$ (LLZTO) solid electrolyte pellet was prepared by combination of solid-state reaction process and hot-pressing sintering as described in our previous reports [31]. Typically, stoichiometric $LiOH{\cdot}H_2O$ (Aladdin Reagent, 99.995%, 15% excess), $La(OH)_3$ (Aladdin Reagent, 99.95%), ZrO_2 (Aladdin Reagent, 99.99%) and Ta_2O_5 (Aladdin Reagent, 99.95%) were mixed and ball-milled followed by calcined at air atmosphere at 950 °C for 12 h to form cubic LLZTO powder. Afterwards, the powder underwent hot-pressing sintering in a carbon die at 1150 °C for 1 h at 20 MPa under Ar atmosphere. The obtained LLZTO ceramic block was finally processed into pellets with 12 mm in diameter and 1 mm in thickness for later use.

2.2. Materials characterization

The phase structures were detected by X-ray diffraction (XRD) using a high-resolution Bruker D8 discover diffractometer equipped with Cu $K_{\alpha 1}$ radiation (λ = 1.5406 Å). The compositions and morphologies were characterized by a JEM-2100F transmission electron microscopy (TEM), and a Hitachi S-4800 scanning electron microscope (SEM) attached with an energy dispersive spectrometer (EDS) and a scanning transmission electron microscopy (STEM). The X-ray photoelectron spectroscopy (XPS) was performed using a Thermo Fisher Scientific ESCAlab 250 spectrometer, and etching was carried out on sample surface by Ar ion beam operating at 2 kV and 1 μA for 10 s.

2.3. Electrochemical measurements and batteries assembly

The ionic conductivity of the LLZTO pellet was determined by a

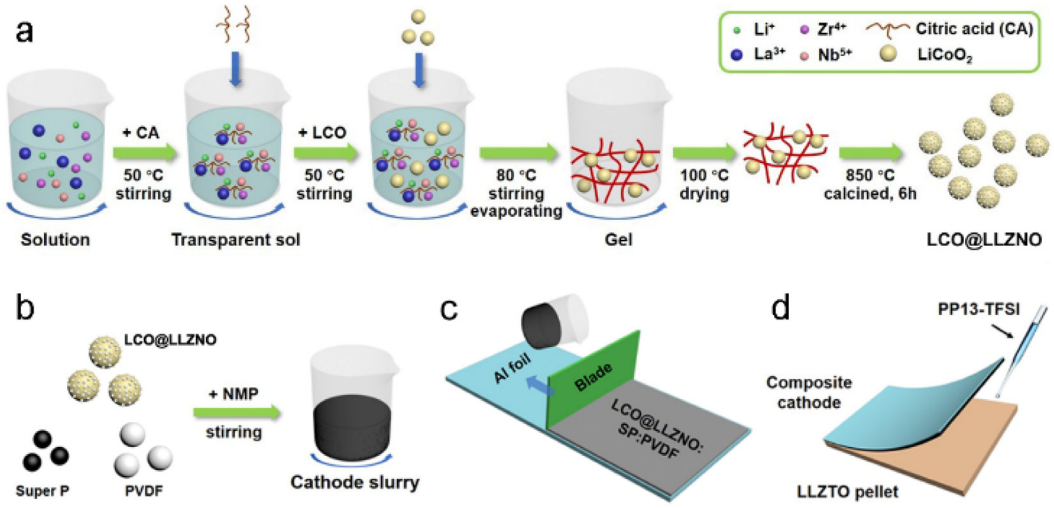

Fig. 1. Schematics of (a) synthesis process of LCO@LLZNO, (b) cathode slurry preparation, (c) cathode electrode preparation by blade casting, and (d) adding PP13-TFSI at cathode-electrolyte interface.

Princeton electrochemical workstation at a frequency range from 7 MHz to 0.1 Hz and a temperature range from 30 to 80 °C with Ag symmetric blocking electrodes. The uniformly mixed cathode slurry of 90 wt% hybrid active material, 5 wt% Super P and 5 wt% PVDF binder in N-methylpyrrolidone (NMP) solvent was casted onto current collector Al foil (Fig. 1b and c). Then the electrode was completely dried at 100 °C in a vacuum oven for 12 h. The active cathode mass loading was ~2 and ~5.2 mg cm^{-2}. The Swagelok-type cell made up of a LCO@LLZNO cathode, a LLZTO solid electrolyte pellet and a Li foil anode was assembled in an Ar-filled glove box (Mikrouna) with O_2 and H_2O contents below 0.1 ppm. Firstly, the LLZTO pellet was polished by SiC sandpapers (successively from 500, 800 to 1000 mesh), and mirror-polished using a diamond polishing slurry (5 and 1 μm). Then, the Li foil was scraped by a scalpel until the bright surface appeared. The bright Li foil was tightly pressed on the polished LLZTO pellet. The LLZTO pellet attached with Li foil was further heated at 180 °C to obtain the good contact between LLZTO pellet and Li foil, followed by cooling to the room temperature for later investigation. Finally, only 1 μL cm^{-2} N-Methyl-N-propylpiperidinium bis(trifluoromethanesulfonyl)imide (PP13-TFSI) ionic liquid was introduced to the interface between the cathode and the LLZTO electrolyte (Fig. 1d). The cyclic voltammetry (CV) and electrochemical impedance spectroscopy (EIS) measurements were carried out using a Princeton electrochemical workstation. Galvanostatic charge-discharge tests were performed using a Land CT2001A cycler within the potential range of 3.0–4.05 V vs Li^+/Li. C-rate values were calculated regarding 115 mAh g^{-1} as the theoretical capacity for $LiCoO_2$ cathode materials [20,32]. All the measurements were carried out at 60 °C.

3. Results and discussion

3.1. Structure and morphology of LCO@LLZNO

Fig. 2a schematically shows that LLZNO nanoparticles are anchored on LCO surface through one-step sol-gel process. X-ray diffraction (XRD) pattern of LLZNO powders that were synthesized using the identical sol-gel method without LCO in precursor is shown in Fig. 2b. All peaks in Fig. 2b are well indexed to cubic garnet phase, indicating that the sol-gel synthesized LLZNO has cubic LLZO structure. Dark-field scanning transmission electron microscopy (STEM) is performed to verify the successful introduction of LLZNO nanocoating (2 wt%) on LCO surface (Fig. 2c). EDS mapping under bright-field STEM mode (Fig. 2d and e) suggests that La, Zr and Nb elements are uniformly distributed on LCO surface. Transmission electron microscopy (TEM) image of LCO@LLZNO (Fig. 2f) reveals that LLZNO coating is comprised of small LLZNO nanoparticles with 40–60 nm in size. Formation of ionically conducting networks between LCO particles through introducing cross-linked LLZNO nano-islands is further detected by STEM (Fig. 2g). Since the LLZO and the LCO can be stable up to 900 °C for more than 10 h [33], the sol-gel processed LLZNO coating on LCO does not affect the hexagonal structure of LCO as demonstrated by XRD scan of LCO@LLZNO (Fig. S1). The clear lattice fringes of 0.32 nm in HR-TEM image for the decoration of LLZNO (Fig. 2h) are well matched with (4 0 0) crystal planes of cubic LLZO, which is consistent with XRD result in Fig. 2b. Such ionically conducting LLZNO coating also reserves spaces for electronic conductive additives. By filling SP into the spaces between LLZNO nanoparticles, SP and LLZNO are homogeneously distributed on LCO surface, and thus cross-linked networks with both high ionic and electronic conduction are built inside the composite cathodes, which are confirmed by the scanning electron microscopy (SEM) and EDS mapping (Figs. S2 and S3).

3.2. Electrochemical performance of solid garnet batteries

LCO or LCO@LLZNO cathodes were prepared by casting slurry consisting of 90 wt% LCO (or LCO@LLZNO), 5 wt% SP and 5 wt% PVDF binder in N-methylpyrrolidone (NMP) solvent onto Al current collector. The Swagelok-type full cell with a LCO@LLZNO cathode, a LLZTO solid electrolyte pellet and a Li foil anode was assembled in an Ar-filled glove box. 1 μL cm^{-2} PP13-TFSI was added between the cathode and the LLZTO electrolyte as an intermediate layer (Fig. S5a). The characterization of LLZTO solid electrolyte is presented in Fig. S4.

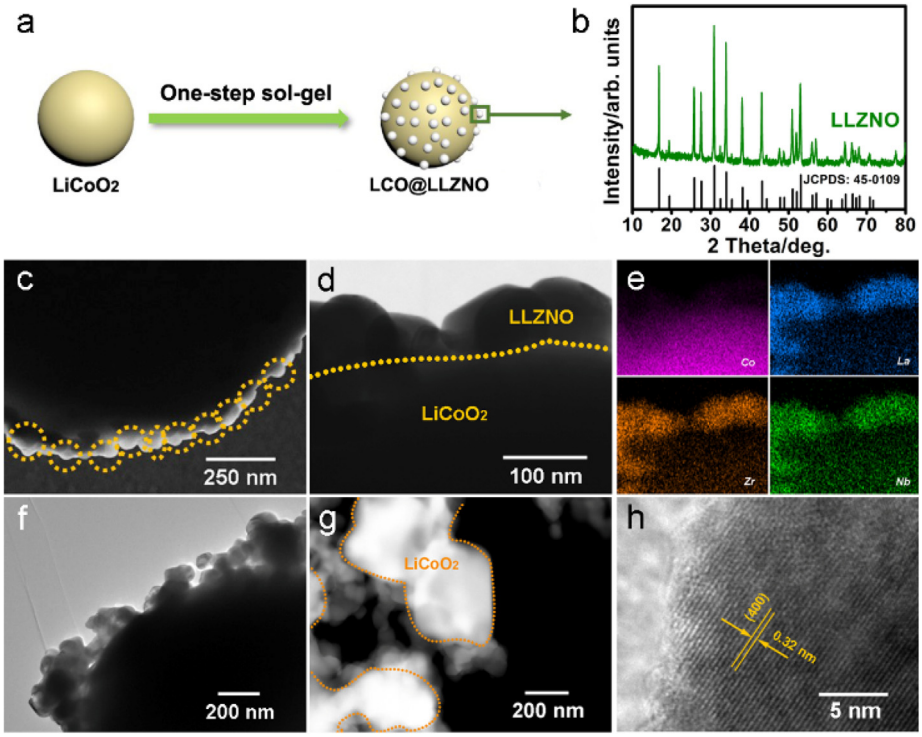

Fig. 2. (a) Schematic structure of LCO@LLZNO. (b) XRD pattern of $Li_{6.375}La_3Zr_{1.375}Nb_{0.625}O_{12}$. (c) Dark-field and (d) bright-field STEM images of LCO@LLZNO. (e) Elemental mapping in area of (d). (f) TEM and (g) STEM images of LCO@LLZNO. (h) HR-TEM image of LLZNO nanocoating.

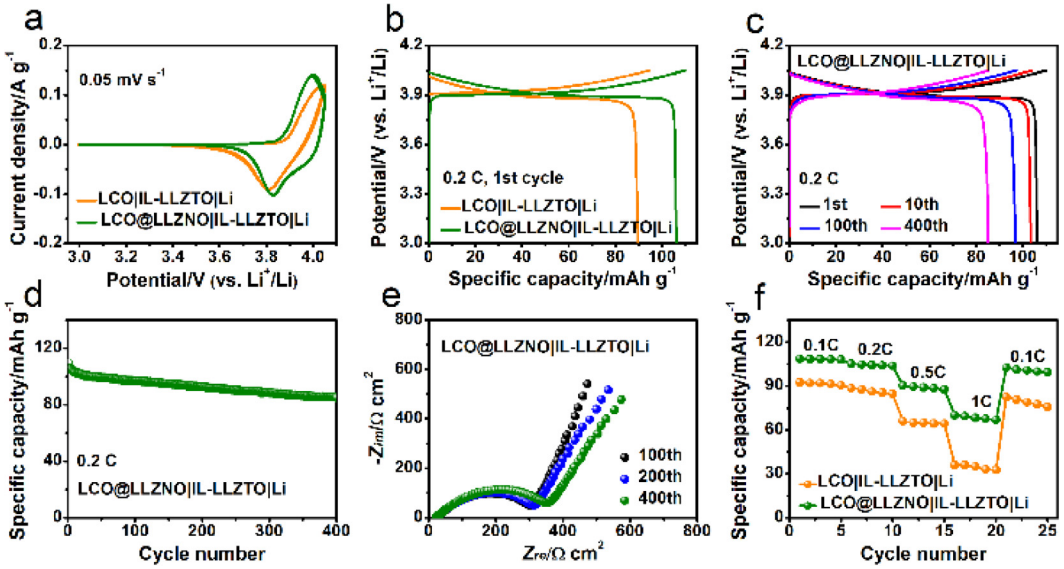

Fig. 3. (a) CV curves of LCO and LCO@LLZNO based batteries. (b) The first charge-discharge curves for two batteries at 0.2 C. (c) Charge-discharge profiles of LCO@LLZNO based battery at 0.2 C. (d) Capacity of LCO@LLZNO based battery during cycling. (e) Nyquist plots of LCO@LLZNO based battery during cycling. (f) Rate performance for two batteries. All the measurements were taken at 60 °C.

Fig. S4a shows the XRD patterns of as-prepared LLZTO powder and hot-pressing sintered LLZTO pellet. It can be clearly seen that the diffraction lines of both LLZTO powder and pellet can be well indexed to a standard cubic garnet phase (JCPDS No. 45-0109), indicating the pure cubic garnet structure of LLZTO solid electrolyte. The ionic conductivity of the LLZTO pellet was measured at a temperature range from 30 to 80 °C and the corresponding Nyquist curves are shown in Fig. S4b. The ionic conductivity of the LLZTO pellet is calculated to be 1.15×10^{-3} S cm^{-1} at 30 °C, and the activation energy E_a is estimated to be 0.27 eV by the fitted Arrhenius plot in Fig. S4c. The electrochemical impedance spectroscopy (EIS) of LCO||Li and LCO@LLZNO||Li cells were further measured (Fig. S5b and c). The interfacial resistance of LCO@LLZNO||Li cell is 1014 Ω cm^2 at room temperature, which is much lower than that (1781 Ω cm^2) of LCO||Li cell. At 60 °C, the interfacial resistance of LCO@LLZNO||Li cell further reduces to 174 Ω cm^2. This can be explained by the good contact between cathodes and electrolytes and 3D ionic/electronic conductive networks in LCO cathode.

Cyclic voltammetry (CV) curve of LCO@LLZNO||Li cell at 0.05 mV s^{-1} in Fig. 3a shows an obvious oxidation peak of ~3.99 V and reduction peak of ~3.83 V, corresponding to the reversible Li^+ de-intercalation and intercalation. By contrast, the LCO||Li cell presents redox peaks at ~4.03 and ~3.81 V, demonstrating a larger potential polarization due to the higher-resistance cathode-electrolyte interface. The first charge and discharge capacities of LCO@LLZNO||Li cell are 109.7 and 106.1 mAh g^{-1}, respectively, while the values for LCO||Li cell are only 94.3 and 89.6 mAh g^{-1} (Fig. 3b). The high capacity for LCO@LLZNO||Li cells is attributed to the 3D cross-linked ionic/electronic conductive networks in the LCO cathode and the good contact between the cathode and the solid electrolyte, significantly facilitating the Li^+ transport. In addition, LCO@LLZNO||Li cell also maintains a stable charge-discharge behavior with a quite small polarization during cycles (Fig. 3c) and a high capacity retention of 80.2% (85.1 mAh g^{-1}) after 400 cycles (Fig. 3d). However, the LCO||Li cell shows a rapid capacity decline within 30 cycles (Fig. S6a). EIS at different cycles (Fig. 3e) indicate that the interfacial resistance of LCO@LLZNO||Li cell slightly increases from initial 174 to 382 Ω cm^2 after 400 cycles. However, the interfacial resistance of uncoated LCO||Li cell sharply increases from 306 to 1376 Ω cm^2 after 30 cycles (Fig. S6b). In addition to high cycle stability, The LCO@LLZNO||Li cell also shows high rate capability (Fig. 3f) with a low polarization even at a high rate of 1C, while the LCO||Li cell shows a much large overpotential at 1 C (Fig. S7). LCO@LLZNO||Li cell maintains a discharge capacity of 70.1 mAh g^{-1} even subjected to 1 C, which is 64.5% of the discharge capacity at 0.1 C (108.6 mAh g^{-1}), while LCO||Li cell delivers a much smaller discharge capacity of 36.0 mAh g^{-1} at 1 C, only 38.9% of the value at 0.1 C (92.6 mAh g^{-1}). The LLZNO coating significantly improves cycle and rate performance, which is attributed to the ionically and electronically conducting networks, and thus the reduced cathode-electrolyte interfacial resistance.

3.3. Mechanism analysis of the interface engineering

X-ray photoelectron spectroscopy (XPS) measurement was taken to analyze the decomposition of PP13-TFSI on LLZTO ctrolyte surface. For noncycled PP13-TFSI, the peak at 688.2 eV is assigned to $–CF_3$ group of $TFSI^-$ (Fig. 4a). The appearance of LiF at 684.5 eV is observed after cycling due to the $TFSI^-$ decomposition. The peaks at 402.0 and 399.0 eV in pristine N 1s spectrum stand for N in $PP13^+$ cation and $TFSI^-$ anion (labeled as N_{cation} and N_{anion}, Fig. 4b). After cycling, the peaks for N_{cation} and N_{anion} are shifted to 401.6 and 398.3 eV, along with the decreased peak intensity ratio of N_{cation} to N_{anion} and the increased full width at half maximum of N_{anion} peak, indicating that $TFSI^-$ degrades and forms Li_3N whose characteristic peak is centered at 396.2 eV [29]. In the case of S 2p spectra (Fig. 4c), the peaks at 169.4 and 168.3 eV are related to $–SO_2–$ group in $TFSI^-$. The evolution of $–SO_2–$ group into polyoxysulfones, polysulfides and Li_2S species during cycling is detected, which is evident from the emerging peaks at 166.8, 162.6 and 161.2–159.0 eV. As for O 1s spectra (Fig. 4d), besides the peak at 532.1 eV for pristine $–SO_2–$ group in $TFSI^-$, two new peaks at 530.9 and 527.8 eV occur after cycling, which are stemmed from decomposing product Li_2O. From XPS study, the decomposition of $TFSI^-$ anion into inorganic products including LiF, Li_3N, Li_2S and Li_2O is observed, in situ generating a solid-state ionically conducting interphase at the cathode-electrolyte interface upon cycling. On the basis of previous literatures [29,34,35], we propose a stepwise decomposition mechanism of $TFSI^-$ during charge/discharge as follows:

$$[(SO_2CF_3)_2N]^-(TFSI^-) + nLi^+ + ne^- \rightarrow Li_2S_2O_4 + Li_3N + LiF + C_2F_xLi_y \quad (1)$$

$$Li_2S_2O_4 + 4Li^+ + 4e^- \rightarrow Li_2SO_3 + Li_2S + Li_2O \quad (2)$$

$$Li_2SO_3 + 6Li^+ + 6e^- \rightarrow Li_2S + 3Li_2O \quad (3)$$

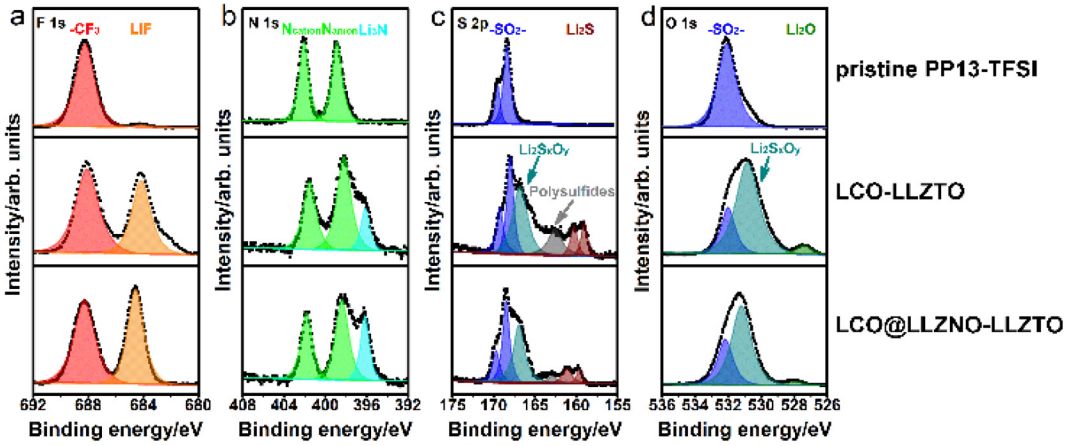

Fig. 4. (a) F 1s, (b) N 1s, (c) S 2p, and (d) O 1s XPS spectra of PP13-TFSI before cycling; LCO-LLZTO and LCO@LLZNO-LLZTO interfaces after cycling.

Constructing such an ionic conductive SEI layer can not only strengthen the physical solid-solid contact, but also reduce the interfacial resistance and improve the cycle stability of solid batteries [36].

The conventional cathode comprised of active material, electronic conductive additive and PVDF binder is directly coupled with a garnet electrolyte (Fig. 5a). Due to poor solid-solid contacts, fluent Li^+ flux is severely inhibited in such cathodes and cathode-electrolyte interfaces, leading to performance degradation [37–39]. Adding PP13-TFSI can reduce the interfacial resistance by constructing an intimate contact between the cathode and the electrolyte (Fig. 5b) [40,41]. In addition, PP13-TFSI can decompose and cause the formation of an ionically conducting interphase by constructing a reactive immediate layer, which facilitates Li^+ transport and stabilizes cathode-electrolyte interface. We further coat the cathode with garnet-typed LLZNO nanoparticles to improve Li^+ transport inside the cathode, forming ionically and electronically conducting networks by cooperating with SP (Fig. 5c). All these interfacial engineering techniques enable the long-life solid garnet batteries. Compared with the rigid sintered interfaces [20,33] or liquid electrolyte modified interfaces [26], at least three benefits can be achieved by adopting the interface engineering strategy presented here: (i) Mixed ionic/electronic conducting networks inside the composite cathode to ensure the optimized cathode capacity; (ii) The in situ formed SEI layer to maintain the good contact between the cathode and the electrolyte during cycles by using the soft PP13-TFSI ionic liquid; (iii) The high safety for solid garnet batteries due to the nonflammable feature of PP13-TFSI ionic liquid.

In addition, the applicable solid batteries need to achieve the breakthrough of energy density to realize commercialization generally by increasing mass loading of cathode materials and use of lighter flexible electrolyte membranes. A preliminary exploration of enlarging cathode mass loading to ~5.2 mg cm^{-2} was taken, and satisfactory results are obtained as presented in Fig. S8 by adopting our interface engineering. Besides, such strategy can be easily extended to electrolyte membranes when the suitable soft and reactive intermediate layer between cathodes and membranes is found out according to the constitution of electrolyte membranes.

4. Conclusion

In conclusion, the 3D cross-linked network with ionic and electronic conduction is constructed inside the composite cathode, and reactive intermediate layer of PP13-TFSI is introduced at the cathode-electrolyte interface. A solid-state ionically conducting interphase is formed by decomposition of anion part in PP13-TFSI, verified by XPS results, which improves the cycle stability of solid garnet batteries. The interface engineering of cathode coating and reactive immediate layer construction is effective to reinforce the cathode-electrolyte interface and feasible to applicable solid batteries.

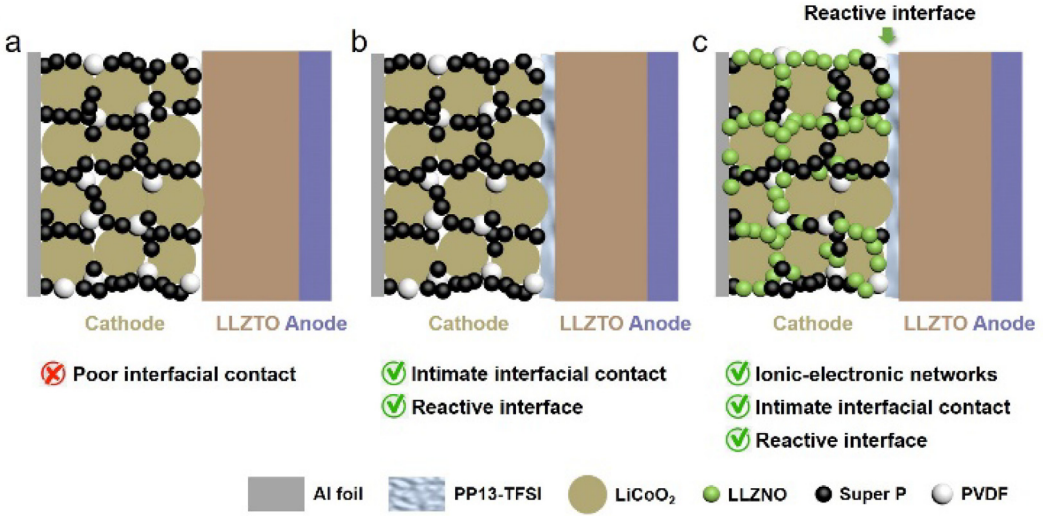

Fig. 5. (a) Illustration of conventional cathode-electrolyte interface. (b) Adding PP13-TFSI at cathode-electrolyte interface. (c) Constructing island-like LLZNO coated cathode, and adding PP13-TFSI at cathode-electrolyte interface.

Declaration of Competing Interest

The authors declare that they have no known competing financial interests or personal relationships that could have appeared to influence the work reported in this paper.

Acknowledgements

This work was supported by the National Key R&D Program of China (Grant No. 2018YFB0104300), the National Natural Science Foundation of China (Grant Nos. 51532002 and 51771222), the National Science Foundation of Shangdong Province (Grant No. ZR201702180185), the China Postdoctoral Science Foundation (Grant No. 2018M632617),and the “Taishan Scholars Program”, and the Project of Qingdao Leading Talents in Entrepreneurship and Innovation.

Appendix A. Supplementary data

Supplementary data to this article can be found online at https://doi.org/10.1016/j.cej.2020.124089.

References

[1] Y. Li, Z. Sun, L. Shi, S. Lu, Z. Sun, Y. Shi, H. Wu, Y. Zhang, S. Ding, Poly(ionic liquid)-polyethylene oxide semi-interpenetrating polymer network solid electrolyte for safe lithium metal batteries, Chem. Eng. J. 375 (2019) 121925.
[2] D. Li, C. Lei, H. Lai, X.-L. Liu, W.-L. Yao, T.-X. Liang, S.-W. Zhong, Recent advancements in interface between cathode and garnet solid electrolyte for all solid state li-ion batteries, J. Inorg. Mater. 34 (2019) 694–702.
[3] C.-B. Li, H.-Y. Yue, Q.-X. Wang, J.-X. Li, S.-T. Yang, Preparation and property of a novel heat-resistant ceramic composite solid-state electrolyte for lithium batteries, J. Inorg. Mater. 32 (2017) 801–805.
[4] W. Zhou, S. Wang, Y. Li, S. Xin, A. Manthiram, J.B. Goodenough, Plating a dendrite-free lithium anode with a polymer/ceramic/polymer sandwich electrolyte, J. Am. Chem. Soc. 138 (2016) 9385–9388.
[5] B. Zhang, L. Chen, J. Hu, Y. Liu, Y. Liu, Q. Feng, G. Zhu, L.-Z. Fan, Solid-state lithium metal batteries enabled with high loading composite cathode materials and ceramic-based composite electrolytes, J. Power Sources 442 (2019) 227230.
[6] S.-S. Chi, Y. Liu, N. Zhao, X. Guo, C.-W. Nan, L.-Z. Fan, Solid polymer electrolyte soft interface layer with 3D lithium anode for all-solid-state lithium batteries, Energy Storage Mater. 17 (2019) 309–316.
[7] X. Chen, W. He, L.-X. Ding, S. Wang, H. Wang, Enhancing interfacial contact in all solid state batteries with a cathode-supported solid electrolyte membrane framework, Energy Environ. Sci. 12 (2019) 938–944.
[8] S. Xu, D.W. McOwen, C. Wang, L. Zhang, W. Luo, C. Chen, Y. Li, Y. Gong, J. Dai, Y. Kuang, C. Yang, T.R. Hamann, E.D. Wachsman, L. Hu, Three-dimensional, solid-state mixed electron-ion conductive framework for lithium metal anode, Nano Lett. 18 (2018) 3926–3933.
[9] X. Tao, Y. Liu, W. Liu, G. Zhou, J. Zhao, D. Lin, C. Zu, O. Sheng, W. Zhang, H.W. Lee, Y. Cui, Solid-state lithium-sulfur batteries operated at 37 degrees C with composites of nanostructured $Li_7La_3Zr_2O_{12}$/carbon foam and polymer, Nano Lett. 17 (2017) 2967–2972.
[10] J. Yi, L. Chen, Y. Liu, H. Geng, L.Z. Fan, High capacity and superior cyclic performances of all-solid-state lithium-sulfur batteries enabled by a high-conductivity $Li_{10}SnP_2S_{12}$ solid electrolyte, ACS Appl. Mater. Interfaces 11 (2019) 36774–36781.
[11] Y. Tian, T. Shi, W.D. Richards, J. Li, J.C. Kim, S.-H. Bo, G. Ceder, Compatibility issues between electrodes and electrolytes in solid-state batteries, Energy Environ. Sci. 10 (2017) 1150–1166.
[12] Z. Yang, H. Yuan, C. Zhou, Y. Wu, W. Tang, S. Sang, H. Liu, Facile interfacial adhesion enabled LATP-based solid-state lithium metal battery, Chem. Eng. J. (2019) 123650, https://doi.org/10.1016/j.cej.2019.123650.
[13] J.Y. Liang, X.X. Zeng, X.D. Zhang, P.F. Wang, J.Y. Ma, Y.X. Yin, X.W. Wu, Y.G. Guo, L.J. Wan, Mitigating interfacial potential drop of cathode-solid electrolyte via ionic conductor layer to enhance interface dynamics for solid batteries, J. Am. Chem. Soc. 140 (2018) 6767–6770.
[14] J. Duan, W. Wu, A.M. Nolan, T. Wang, J. Wen, C. Hu, Y. Mo, W. Luo, Y. Huang, Lithium-graphite paste: an interface compatible anode for solid-state batteries, Adv. Mater. 31 (2019) 1807243.
[15] N. Delaporte, A. Guerfi, H. Demers, H. Lorrmann, A. Paolella, K. Zaghib, Facile protection of lithium metal for all-solid-state batteries, ChemistryOpen 8 (2019) 192–195.
[16] A. Mauger, C.M. Julien, A. Paolella, M. Armand, K. Zaghib, Building better batteries in the solid state: a review, Materials 12 (2019) 3892.
[17] N. Zhao, W. Khokhar, Z. Bi, C. Shi, X. Guo, L.-Z. Fan, C.-W. Nan, Solid garnet batteries, Joule 3 (2019) 1190–1199.
[18] C. Wang, L. Zhang, H. Xie, G. Pastel, J. Dai, Y. Gong, B. Liu, E.D. Wachsman, L. Hu, Mixed ionic-electronic conductor enabled effective cathode-electrolyte interface in all solid state batteries, Nano Energy 50 (2018) 393–400.
[19] B. Liu, Y. Gong, K. Fu, X. Han, Y. Yao, G. Pastel, C. Yang, H. Xie, E.D. Wachsman, L. Hu, Garnet solid electrolyte protected Li-metal batteries, ACS Appl. Mater. Interfaces 9 (2017) 18809–18815.
[20] F. Han, J. Yue, C. Chen, N. Zhao, X. Fan, Z. Ma, T. Gao, F. Wang, X. Guo, C. Wang, Interphase engineering enabled all-ceramic lithium battery, Joule 2 (2018) 497–508.
[21] Y.-F. Deng, S.-X. Zhao, Y.-H. Xu, C.-W. Nan, Effect of temperature of Li_2O-Al_2O_3-TiO_2-P_2O_5 solid-state electrolyte coating process on the performance of $LiNi_{0.5}Mn_{1.5}O_4$ cathode materials, J. Power Sources 296 (2015) 261–267.
[22] K. Bi, S.-X. Zhao, C. Huang, C.-W. Nan, Improving low-temperature performance of spinel $LiNi_{0.5}Mn_{1.5}O_4$ electrode and $LiNi_{0.5}Mn_{1.5}O_4$/$Li_4Ti_5O_{12}$ full-cell by coating solid-state electrolyte Li-Al-Ti-P-O, J. Power Sources 389 (2018) 240–248.
[23] L.-P. Wang, X.-D. Zhang, T.-S. Wang, Y.-X. Yin, J.-L. Shi, C.-R. Wang, Y.-G. Guo, Ameliorating the interfacial problems of cathode and solid-state electrolytes by interface modification of functional polymers, Adv. Energy Mater. 8 (2018) 1801528.
[24] T. Wang, W. Wang, D. Zhu, L. Huang, Y. Chen, Improvement of the overall performances of $LiMn_2O_4$ via surface-modification by polypyrrole, Mater. Res. Bull. 71 (2015) 91–97.
[25] E. Umeshbabu, B. Zheng, J. Zhu, H. Wang, Y. Li, Y. Yang, Stable cycling lithium-sulfur solid batteries with enhanced Li/$Li_{10}GeP_2S_{12}$ solid electrolyte interface stability, ACS Appl. Mater. Interfaces 11 (2019) 18436–18447.
[26] C.-Z. Zhao, B.-C. Zhao, C. Yan, X.-Q. Zhang, J.-Q. Huang, Y. Mo, X. Xu, H. Li, Q. Zhang, Liquid phase therapy to solid electrolyte–electrode interface in solid-state Li metal batteries: a review, Energy Storage Mater. (2019), https://doi.org/10.1016/j.ensm.2019.07.026.
[27] H.W. Kim, P. Manikandan, Y.J. Lim, J.H. Kim, S.-C. Nam, Y. Kim, Hybrid solid electrolyte with the combination of $Li_7La_3Zr_2O_{12}$ ceramic and ionic liquid for high voltage pseudo-solid-state Li-ion batteries, J. Mater. Chem. A 4 (2016) 17025–17032.
[28] A. Mauger, C.M. Julien, A. Paolella, M. Armand, K. Zaghib, A comprehensive review of lithium salts and beyond for rechargeable batteries: Progress and perspectives, Mater. Sci. Eng., R 134 (2018) 1–21.
[29] J.E. Morales-Ugarte, E. Bolimowska, H. Rouault, J. Santos-Peña, C.C. Santini, A. Benayad, EIS and XPS investigation on SEI layer formation during first discharge on graphite electrode with a vinylene carbonate doped imidazolium based ionic liquid electrolyte, J. Phys. Chem. C 122 (2018) 18223–18230.
[30] J.B. Haskins, H. Yildirim, C.W. Bauschlicher, J.W. Lawson, Decomposition of ionic liquids at lithium interfaces. 2. Gas phase computations, J. Phys. Chem. C 121 (2017) 28235–28248.
[31] F. Du, N. Zhao, Y. Li, C. Chen, Z. Liu, X. Guo, All solid state lithium batteries based on lamellar garnet-type ceramic electrolytes, J. Power Sources 300 (2015) 24–28.
[32] S. Ohta, S. Komagata, J. Seki, T. Saeki, S. Morishita, T. Asaoka, All-solid-state lithium ion battery using garnet-type oxide and Li_3BO_3 solid electrolytes fabricated by screen-printing, J. Power Sources 238 (2013) 53–56.
[33] C.-L. Tsai, Q. Ma, C. Dellen, S. Lobe, F. Vondahlen, A. Windmüller, D. Grüner, H. Zheng, S. Uhlenbruck, M. Finsterbusch, F. Tietz, D. Fattakhova-Rohlfing, H.P. Buchkremer, O. Guillon, A garnet structure-based all-solid-state Li battery without interface modification: resolving incompatibility issues on positive electrodes, Sustainable Energy Fuels 3 (2019) 280–291.
[34] D. Aurbach, A. Zaban, Y. Ein-Eli, I. Weissman, O. Chusid, B. Markovsky, M. Levi, E. Levi, A. Schechter, E. Granot, Recent studies on the correlation between surface chemistry, morphology, three-dimensional structures and performance of Li and Li-C intercalation anodes in several important electrolyte systems, J. Power Sources 68 (1997) 91–98.
[35] C. Xu, B. Sun, T. Gustafsson, K. Edström, D. Brandell, M. Hahlin, Interface layer formation in solid polymer electrolyte lithium batteries: an XPS study, J. Mater. Chem. A 2 (2014) 7256–7264.
[36] B. Zheng, J. Zhu, H. Wang, M. Feng, E. Umeshbabu, Y. Li, Q.H. Wu, Y. Yang, Stabilizing $Li_{10}SnP_2S_{12}$/Li interface via an in situ formed solid electrolyte interphase layer, ACS Appl. Mater. Interfaces 10 (2018) 25473–25482.
[37] M. He, Z. Cui, C. Chen, Y. Li, X. Guo, Formation of self-limited, stable and conductive interfaces between garnet electrolytes and lithium anodes for reversible lithium cycling in solid-state batteries, J. Mater. Chem. A 6 (2018) 11463–11470.
[38] J. Zhang, N. Zhao, M. Zhang, Y. Li, P.K. Chu, X. Guo, Z. Di, X. Wang, H. Li, Flexible and ion-conducting membrane electrolytes for solid-state lithium batteries: dispersion of garnet nanoparticles in insulating polyethylene oxide, Nano Energy 28 (2016) 447–454.
[39] A. Aboulaich, R. Bouchet, G. Delaizir, V. Seznec, L. Tortet, M. Morcrette, P. Rozier, J.-M. Tarascon, V. Viallet, M. Dollé, A new approach to develop safe all-inorganic monolithic Li-ion batteries, Adv. Energy Mater. 1 (2011) 179–183.
[40] Z. Zhang, Q. Zhang, J. Shi, Y.S. Chu, X. Yu, K. Xu, M. Ge, H. Yan, W. Li, L. Gu, Y.-S. Hu, H. Li, X.-Q. Yang, L. Chen, X. Huang, A Self-forming composite electrolyte for solid-state sodium battery with ultralong cycle life, Adv. Energy Mater. 7 (2017) 1601196.
[41] M.R. Busche, T. Drossel, T. Leichtweiss, D.A. Weber, M. Falk, M. Schneider, M.L. Reich, H. Sommer, P. Adelhelm, J. Janek, Dynamic formation of a solid-liquid electrolyte interphase and its consequences for hybrid-battery concepts, Nat. Chem. 8 (2016) 426–434.